Medusae Fossae Formation: New perspectives from Mars Global Surveyor

Bethany A. Bradley[1] and Susan E. H. Sakimoto
GEST at the Geodynamics Branch, NASA Goddard Space Flight Center, Greenbelt, Maryland, USA

Herbert Frey
Geodynamics Branch, NASA Goddard Space Flight Center, Greenbelt, Maryland, USA

James R. Zimbelman
CEPS/National Air and Space Museum, Smithsonian Institution, Washington, D. C., USA

Received 5 July 2001; revised 28 November 2001; accepted 3 December 2001; published 17 August 2002.

[1] The nature and origin of the Medusae Fossae Formation (MFF) on Mars has been debated since the return of the first Viking images. The MFF's young age, distinctive surface texture, and lack of obvious source have prompted multiple hypotheses for its origin. This study uses data from the Mars Global Surveyor (MGS) mission to examine the MFF at all available scales. We discuss and quantify observations from Mars Orbiter Laser Altimeter (MOLA) topography and Mars Orbiter Camera (MOC) images to better constrain the origin of the MFF. Topographic grid estimates yield a present extent of 2.1×10^6 km^2 and a volume of 1.4×10^6 km^3; however, remnant yardang deposits observed far from the thicker lobes of MFF material suggest that it may have once covered up to 5×10^6 km^2. We do not find compelling evidence for extensive fluvial reworking of the MFF; however, in several regions, buried channels are apparent in the MFF because the formation is draped over underlying topography. Layering is apparent at all scales, from submeter to hundreds of meters, with variable resistance to weathering. Continuity of layers appears to be local to regional, but not likely formation-wide. Yardangs form both parallel and bidirectional patterns, with resistant layers and jointing probably influencing their orientations. A comparative study of MFF regional topography and surface expression indicates that the MFF is quantitatively dissimilar to Martian polar layered deposits. The material is most likely a friable and irregularly consolidated air fall deposit of probable volcanic origin. *INDEX TERMS:* 5470 Planetology: Solid Surface Planets: Surface materials and properties; 5480 Planetology: Solid Surface Planets: Volcanism (8450); *KEYWORDS:* Mars, Medusae Fossae Formation, Mars Global Surveyor, layering, volcanism

1. Introduction

[2] The Medusae Fossae Formation (MFF) is an extensive, geologically young, wind-scoured deposit located near Mars' equator from 130° to 240°E and 15°S to 15°N, between the Tharsis and Elysium volcanic centers. The MFF is one of the youngest units in this area [*Scott and Tanaka*, 1986; *Greeley and Guest*, 1987], overlying both Noachian cratered highland and Amazonian lowland terrain [*Bradley and Sakimoto*, 2001a]. In Elysium Planitia the MFF overlies young volcanic units and small cones [*Lanagan et al.*, 2001] which may be part of a sequence of flows dated as young as 10 Ma [*Hartmann and Berman*, 2000]. Elysium lava interaction with near-surface volatiles would have produced a substantial volume of pyroclastic material [*Keszthelyi et al.*, 2000] and may be a potential source for the MFF. In images the MFF generally appears smooth at large scales, particularly in eastern deposits and where it lies within the "stealth" radar region [*Edgett et al.*, 1997]. Western deposits, located south of Elysium Mons, are much thinner than elsewhere and tend to look rougher because basement material is only partially buried [*Bradley et al.*, 2000]. At a smaller scale the surface of the MFF consists of lineations interpreted to be wind-eroded yardangs [*Ward*, 1979; *El-Baz et al.*, 1979; *Scott and Tanaka*, 1982]. Surface roughness as calculated by Mars Orbiter Laser Altimeter (MOLA) pulse width is 2–3 times greater than the typical Martian surface, presumably owing to the ubiquitous presence of yardangs [*Sakimoto et al.*, 1999].

[3] Variations in surface appearance along with a lack of obvious source have resulted in numerous hypotheses for the formation of the MFF. The proposed origins based on Viking data include ignimbrites or ash flows [*Malin*, 1979; *Scott*

[1]Now at Department of Geological Sciences, Brown University, Providence, Rhode Island, USA.

0148-0227/02/2001JE001537$09.00

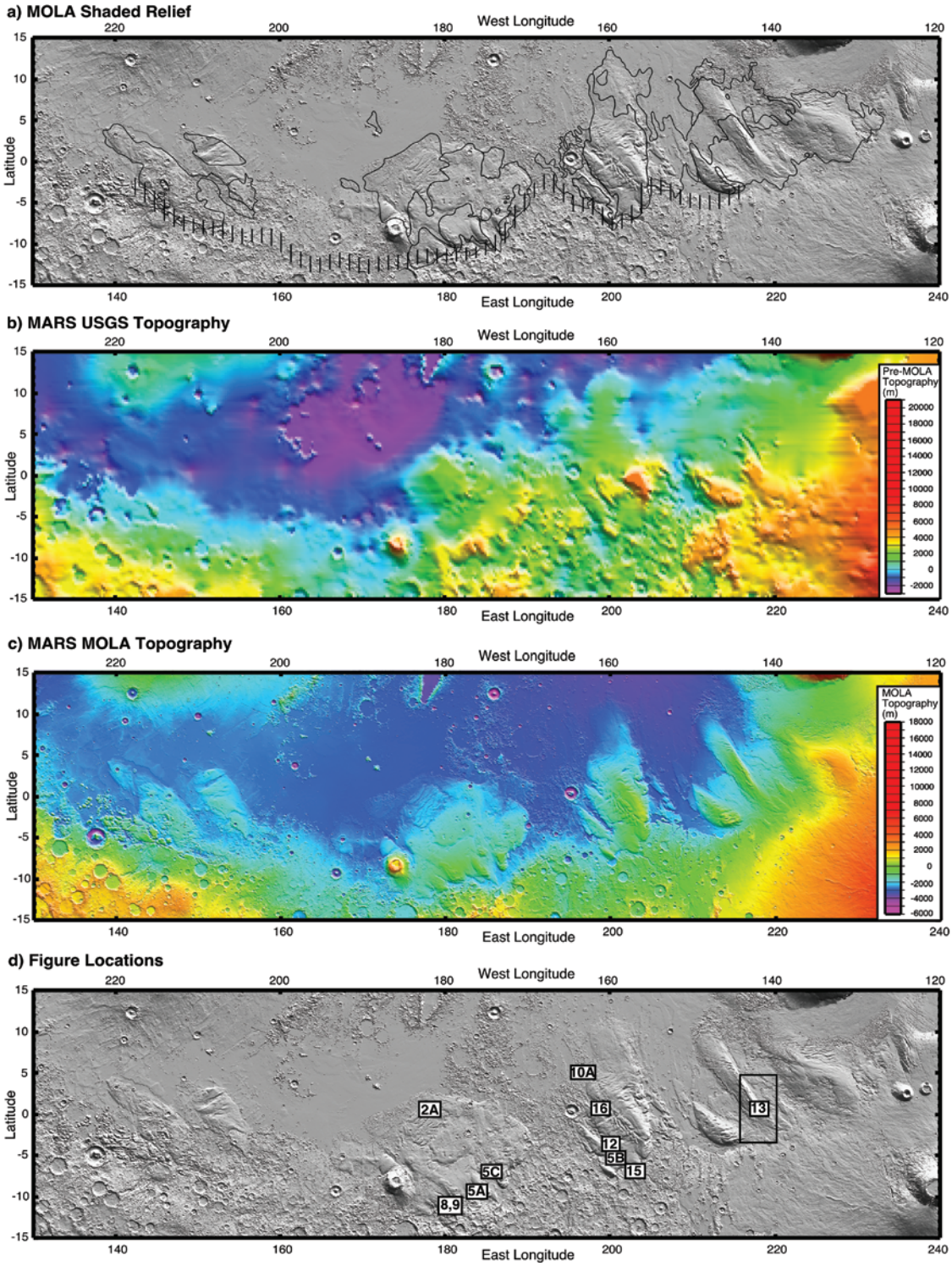

Figure 1. (a) MOLA shaded relief map of the Medusae Fossae Formation. Solid lines are MFF geologic boundaries, and the dashed line represents the dichotomy boundary as mapped by *Scott and Tanaka* [1986] and *Greeley and Guest* [1987]. (b) Pre-MOLA topography according to the U.S. Geological Survey (USGS). (c) MOLA topography with resolution of 32 pixels/degree. Note that MFF elevation, and therefore thickness, was vastly overestimated in USGS topography maps. (d) Location map for areas described in this paper with numbers corresponding to figures. MOLA topography used for this investigation uses an areocentric latitude convention.

and Tanaka, 1982; *Zimbelman et al.*, 1997a], carbonate platforms [*Parker*, 1991], shoreline terraces [*Rice et al.*, 1997], rafted pumice deposits [*Mouginis-Mark*, 1993], paleopolar deposits [*Schultz and Lutz*, 1988; *Head*, 2000], and uplifted and exhumed Noachian terrain [*Forsythe and Zimbelman*, 1988]. Recent work using Mars Global Surveyor's (MGS's) MOLA and Mars Orbiter Camera (MOC) data narrows the most likely options to two: volcanic air fall and eolian deposits [*Zimbelman et al.*, 1997a; *Sakimoto et al.*, 1999; *Tanaka*, 2000]. Because these two origins imply vastly different recent conditions on Mars, we attempt to differentiate between them and other proposed origins with more confidence and recalculate the area and volume of the deposit. MOLA and MOC data are used to quantitatively examine several aspects of the MFF, including layering, yardang relationships and possible jointing, and MFF interaction with fluvial channels. We discuss the implications for a volcanic air fall versus eolian origin and also reexamine the recently reproposed polar origin hypothesis [*Head*, 2000] using a quantitative comparison of valley geometries.

[4] Global geologic mapping prior to the MGS mission identified three distinct sections of MFF described as upper, middle, and lower members [*Scott and Tanaka*, 1986; *Greeley and Guest*, 1987]. More recent work using MOLA found that mapped members are poorly matched to topographic breaks, indicating that the regional structure and layering are more complex than could originally be determined using Viking data alone [*Sakimoto et al.*, 1999]. Regional mapping at the 1:500,000 scale has also shown that multiple layers (many tens of meters thick) exist, consisting of cohesive caprock overlying more friable material [*Zimbelman et al.*, 1996a, 1997b, 1998].

[5] *Wells and Zimbelman* [1997] noted several regions where layering in the MFF is associated with changing yardang trends. In some areas, exhumed lower layers contain yardangs oriented nearly perpendicular to those on the present surface. This was interpreted to imply multiple stages of eolian erosion with wind regimes varying from layer to layer. Elsewhere, it was observed that yardangs visible in Viking images are not aligned with the prevailing wind direction. This indicates that either many wind regimes have affected the MFF or that the MFF has some structural characteristics such as jointed or welded layers that affect the orientation of the yardangs [*Scott and Tanaka*, 1982, 1986; *Tanaka and Golombek*, 1989]. Resistant layers and possible joints have also become apparent in MOC images, prompting further exploration of yardang expression [*Bradley and Sakimoto*, 2001b]. Here we investigate the occurrence of changing yardang directions and their relationship to topography. We also explore the possibility that jointing within resistant layers causes some of the strange yardang patterns and orientation changes seen in both Viking and MOC images.

[6] Two facets of the MFF that are better illustrated with MGS data are the effect of underlying topography on the MFF appearance and the interaction of the MFF with fluvial processes. In many regions of the MFF, basement peaks and valleys are still visible at the surface with the MFF draped on top of, but not fully masking, underlying features [*Sakimoto et al.*, 1999; *Bradley et al.*, 2000; *Zimbelman et al.*, 2000]. It is this aspect that most convincingly supports an airborne origin.

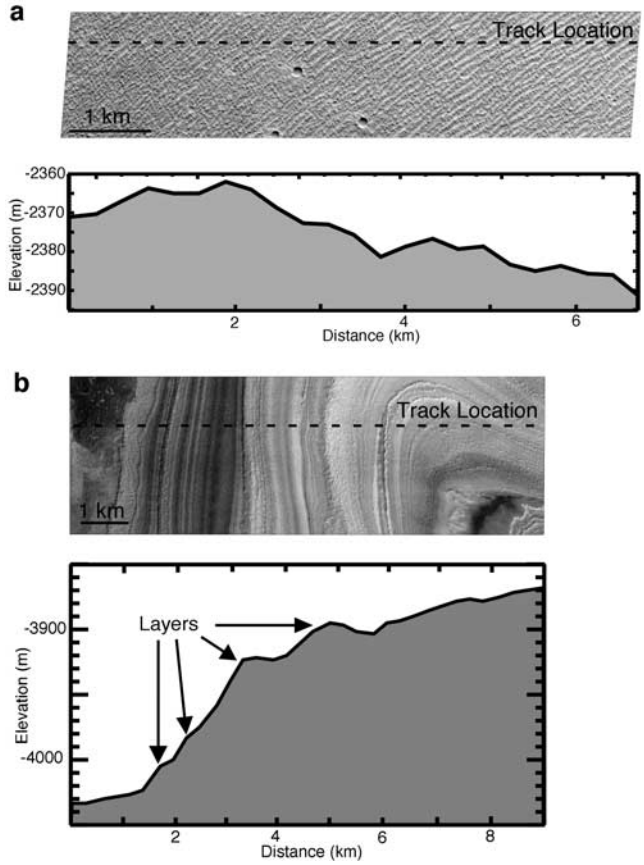

Figure 2. (a) MOC image M0201173 of MFF "ridge and valley" region with corresponding MOLA pass 11150. The image is centered at 177.5°E, 0.83°S. Typical of all MOC images in the "ridge and valley" region, this image shows abundant yardangs but no indication of small-scale layering. The dashed line indicates MOLA track location; the MOLA topography has a vertical exaggeration of 50. Illumination is from the southwest. (b) MOC image M0204019 of northern polar layered deposits with corresponding MOLA pass 11333. The image is centered at 290.95°E, 83.21°N. This image is typical of polar layered terrain and shows a series of small-scale layers but contains no wind-carved features such as yardangs. The dashed line indicates MOLA track location; MOLA topography has a vertical exaggeration of 25. Illumination is from the northeast. (MOC image courtesy of NASA/JPL/MSSS.)

[7] *Zimbelman et al.* [2000] noted a subtle topographic channel originating on the western flank of Arsia Mons that eventually intersects and appears to be diverted by MFF material, making the interrelationship between the MFF and fluvial processes more complex than previously thought. While we find no evidence for large-scale fluvial interaction elsewhere, some localized flow may postdate the MFF near Nicholson crater as well as southeast of Apollineras Patera [*Bradley and Sakimoto*, 2001a]. We further explore the MFF deposit east of Nicholson crater for evidence of fluvial interaction.

[8] Finally, we use MOLA data to estimate the area and volume of MFF material now present in these deposits. *Scott and Tanaka* [1982] estimated that the MFF covered

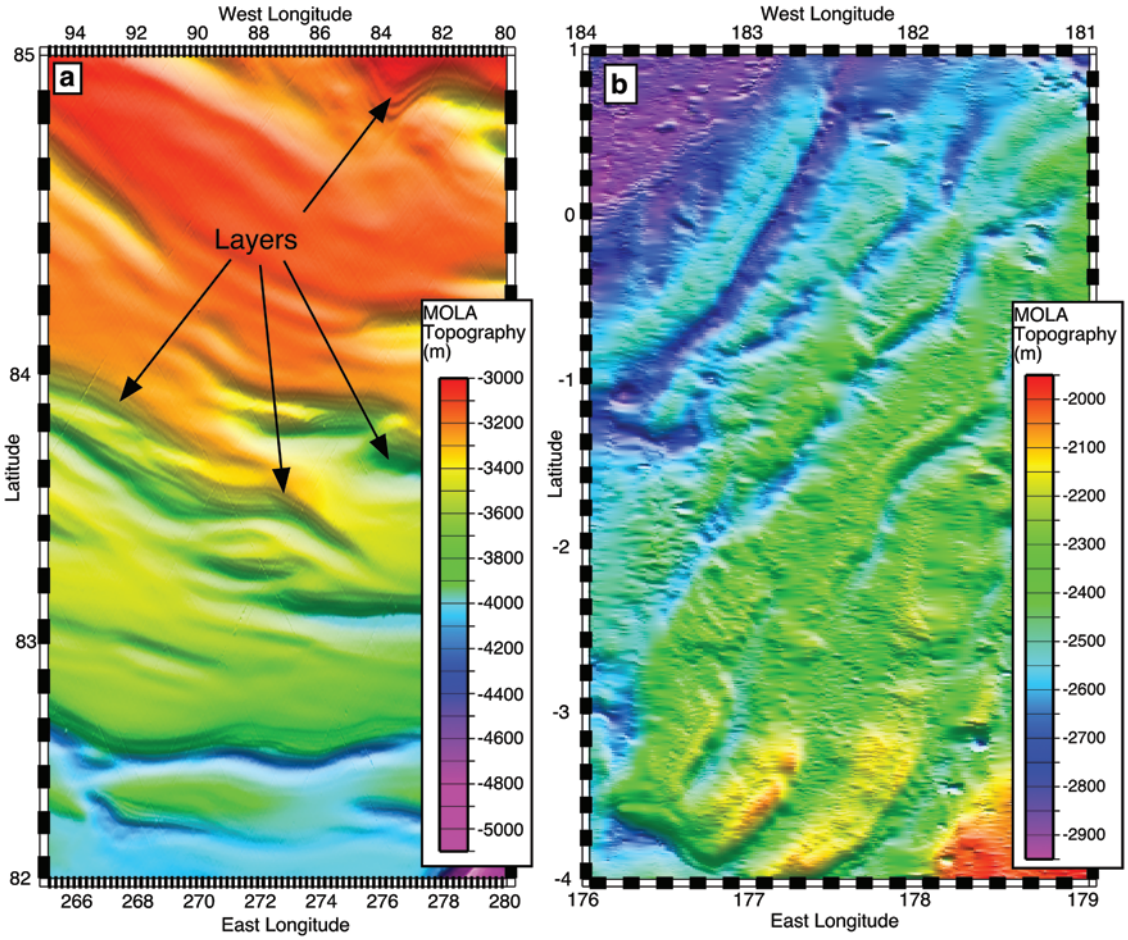

Figure 3. (a) MOLA DEM shows the presence of small-scale layers in north polar layered terrain. DEM resolution is 256 pixels/degree latitudinally and 64 pixels/degree longitudinally. MOLA data through February 2001. (b) MOLA DEM of the MFF ridge and valley region does not reveal the presence of small-scale layering. DEM resolution is 256 pixels/degree latitudinally and 64 pixels/degree longitudinaly. MOLA data through February 2001.

2.2×10^6 km^2 and contained a volume of material of at least 3.85×10^6 km^3 (Figure 1). This volume estimate was based on an MFF thickness of up to 3 km. MOLA topography has since shown the deposit to be locally much thinner and therefore less voluminous [*Smith et al.*, 1999; *Sakimoto et al.*, 1999]. Later work using MOLA aerobraking tracks produced area and volume measurements of 2.5×10^6 km^2 and 1×10^6 km^3, respectively [*Tanaka*, 2000]. In this work we also estimate the total area that the MFF may have once covered on the basis of the presence of yardangs in MOC images.

2. Comparison of Medusae Fossae Formation to Polar Layered Terrain

2.1. MOC Textures and Layers

[9] It has been suggested that the Medusae Fossae Formation is composed of polar layered deposits formed from polar wandering occurring before the onset of Tharsis volcanism [*Schultz and Lutz*, 1988]. This study cited the formation's thickness, the presence of exhumed impact basins, and the possibility of small-scale layering in some Viking images as evidence for an ice-depositional origin. *Head* [2000] reproposed this idea on the basis of MOLA digital elevation models (DEMs) which reveal that one section of the MFF has grossly similar topographic characteristics to polar layered terrain. *Head*'s [2000] suggested region, located between 5°S and 2°N and 175°E and 180°E, contains a series of near-parallel ridges and valleys running perpendicular to the regional gradient, a pattern reminiscent of that seen in polar layered terrain. If the MFF is polar layered terrain, then this ridge and valley system would presumably contain thin layered deposits like those found at the edges of both polar caps and should display topographic characteristics similar to polar layered terrain when subsequent erosion is taken into account. Therefore we quantitatively compare the topography of the MFF region suggested by *Head* [2000] to a sample region of typical north polar layered terrain [*Bradley and Sakimoto*, 2000].

[10] Specifically, we compare the MFF region from 5°S to 2°N and 175°E to 180°E, which we call the MFF "ridges and valleys," to a typical polar region located between 81° and 84°N and 79° and 91°E using MOC images, MOLA profile data, and gridded MOLA topography. We created

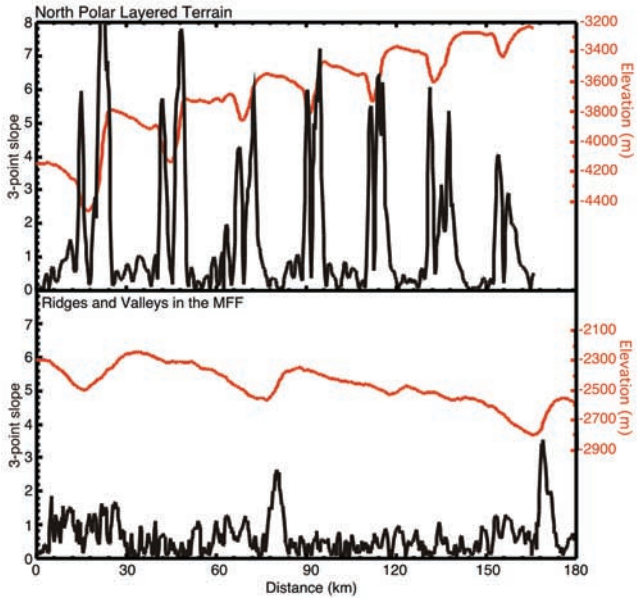

Figure 4. These graphs compare (top) MOLA pass 10134 through north polar layered terrain and (bottom) MOLA pass 11150 through the MFF Ridge and Valley region. MOLA passes (shown in red) cover a distance of 180 km and have a vertical exaggeration of 50. Polar valleys are narrower, are more closely spaced, and have a higher three-point valley wall slope (shown in black) than MFF valleys.

MOLA DEMs using the crossover correction approach of *Neumann et al.* [2001]. In this study we use a default resolution of 64 pixels per degree longitude by 256 pixels per degree latitude (approximately 1 by 0.25 km) unless otherwise stated.

2.2. Images of Small-Scale Textures and Layering

[11] On the smallest scale our survey of the nine currently released MOC images in the MFF "ridge and valley" region reveals that the terrain at a 1–2 m/pixel resolution consists of parallel yardangs. The surface expression of the MFF in this region is typified by MOC image M0201173 (Figure 2a), showing northwest trending yardangs oblique to the valley slope. In contrast, an examination of a typical MOC image in polar terrain (Figure 2b) shows the prevalent expression of multiple thin layers. In fact, MOC images of the poles frequently reveal a variety of layer textures [e.g., see *Malin and Edgett*, 2001, Figures 66–71] and other features, but so far none that appear similar to MFF yardangs and lineations. There is no indication in the MOC images of the MFF region of small-scale layering (polar-like or otherwise), despite good image coverage of several valley walls. While some MOC images within the MFF do reveal layering (see later sections), they generally look quite different than the layers seen in the polar regions and are located within MFF regions where the gross topographic characteristics are markedly different than that of the polar layered terrain.

2.3. Topographic Tests of Small-Scale Layering

[12] High-resolution MOLA DEMs are another effective tool for detecting small-scale layering. Layers apparent in MOLA DEMs occur in both north and south polar deposits and often are continuous for tens of kilometers. Although MOLA coverage in equatorial regions is not as finely spaced longitudinally as in the polar regions, layering was apparent in polar DEMs even early in the mission [e.g., *Zuber et al.*, 1998], when longitudinal coverage was similar to that now available for the equatorial regions. Current DEM resolution, aided by examination of individual MOLA passes, would reveal this same type of layering in the MFF region, if it were present. Our DEMs of the ridge and valley region of MFF show that valley walls do not contain the topographic breaks reminiscent of layering found ubiquitously in polar layered terrain (Figure 3). Additionally, topographic breaks in individual MOLA passes (see Figure 2) are not continuous to adjacent MOLA passes and are thus better attributed to surface roughness.

2.4. Topographic Characterization of Valley Geometry

[13] A quantitative comparison of geometries of the ridge and valley region and our example area containing typical polar layered terrain is readily accomplished using individual MOLA passes. We measure dimensions of valleys located within these regions and calculate three-point average slopes of valley walls. Figure 4 shows the result from representative MOLA passes 10134 of polar terrain and 11150 of MFF. Because MOLA pass 11150 is not quite perpendicular to MFF ridges and valleys, we measure the angle between the MOLA pass and the line perpendicular to ridgelines to derive maximum slopes for the region. Several significant differences are readily apparent. The average MFF valley is 26.4 km wide and 256 m deep and has a valley wall slope of 1.5°–2.5°, while the average polar valley is 9.4 km wide and 380 m deep and has a valley wall slope of 3°–4° (Table 1). The MFF shows greater small-scale roughness between valleys than seen in polar terrain based on changes in MOLA point to point slope. North polar valleys are evenly spaced 25–30 km apart, while MFF valley spacing ranges from 45 to 90 km. Polar valleys show a peak slope of nearly 11°, while MFF valleys reach a maximum of 5°. The underlying regional gradient measured from peak to peak and valley to valley in the MFF averages 0.10°, while regional gradient under the polar layered terrain averages 0.37°.

2.5. Polar Comparison Summary

[14] An analysis of MOC images and MOLA topography in the ridge and valley region of the MFF shows that it is not very similar to typical polar layered terrain. Despite some-

Table 1. Comparison of Valley Attributes

	Medusae Fossae Formation	Northern Polar Layers
Surface features in MOC	yardangs no small-scale layers	small-scale layers, no yardangs
Surface features in MOLA DEM	no layers	small scale layers
Average valley width, km	26.4 ± 5.5	9.4 ± 1.4
Average valley depth, m	256 ± 54	380 ± 122
Spacing between valleys, km	45–90	25–30
Average valley slope, deg	1.5–2.5	3–4
Maximum valley slope, deg	5 ± 0.5	11 ± 0.2
Regional gradient, deg	0.10	0.37

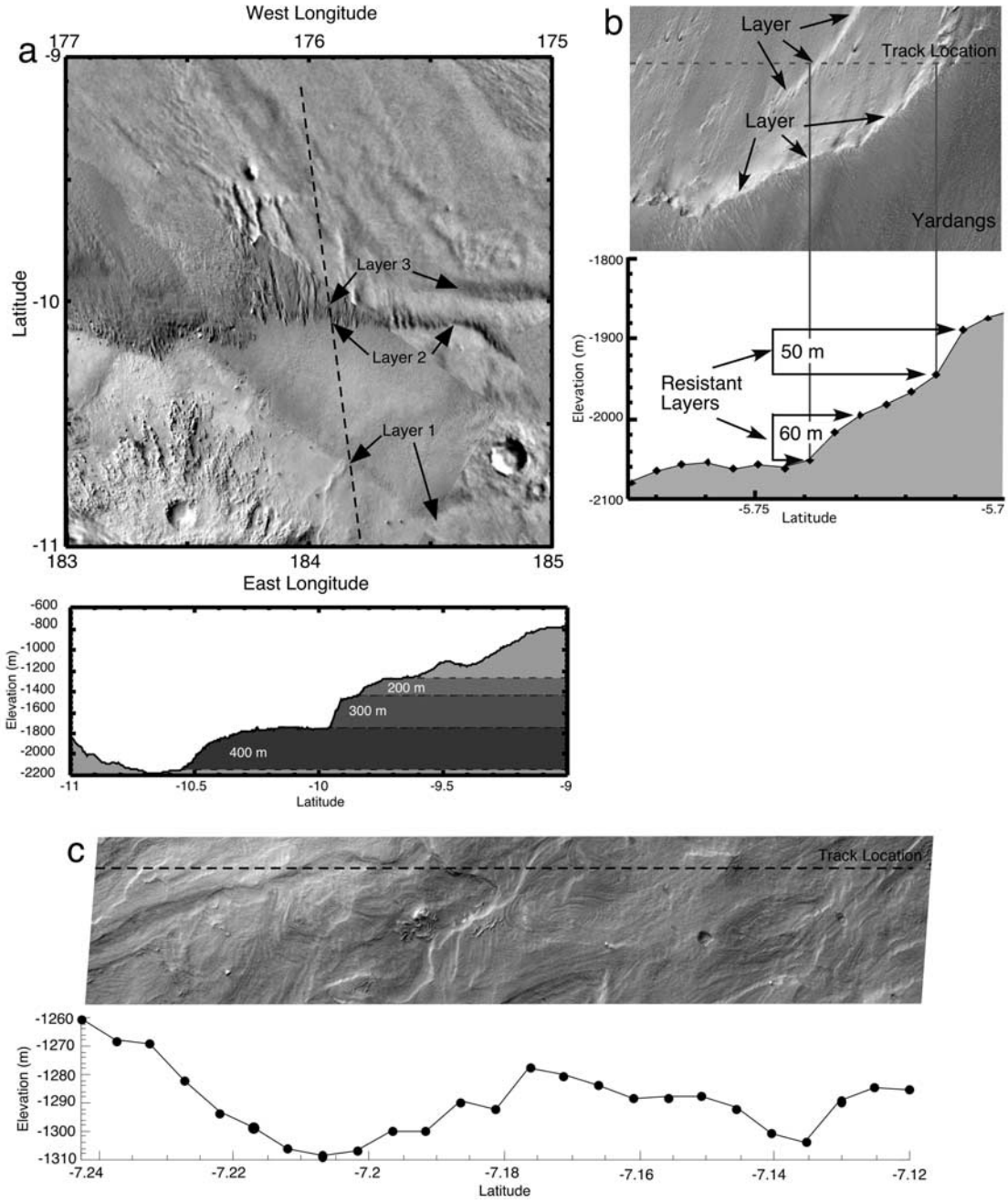

Figure 5. (a) Large-scale layering is apparent in the Viking Mars Digital Image Mosaic (MDIM) and in Viking high-resolution images 439S01 and 439S02 (resolution 65 m/pixel). Dashed line indicates the track location of MOLA pass 10672 through these layers. The graph of MOLA topography has a vertical exaggeration of 25. The MOLA pass shows at least three resistant layers in this region. (b) MOC image M1201209 shows two resistant layers in the MFF underlying a wind-carved friable layer. MOLA pass 14161 shows the presence of the two 50–60 m layers. The graph has a vertical exaggeration of 10. Illumination is from the southwest. (c) MOC image M1101107 shows small-scale layering in the MFF. The image is centered at 7.28°S, 182.97°E and has a resolution of 2.85 m/pixel. The corresponding MOLA pass 13732 does not resolve these layers. The graph has a vertical exaggeration of 25. Illumination is from the southwest. (MOC image courtesy of NASA/JPL/MSSS.)

what similar Viking image appearance and gross regional topographic characteristics, upon close examination, the small-scale image features, topographic layering, and valley geometry are demonstrably quite different. MOC images at 1–2 m/pixel clearly resolve the ubiquitous presence of yardangs on the MFF surface but show no evidence of layering in the area identified by *Head* [2000]. Further, MOLA DEMs of the ridge and valley region reveal valley walls to be rough but without layers. Erosion may account for some shallowing of valleys and lessening of slopes;

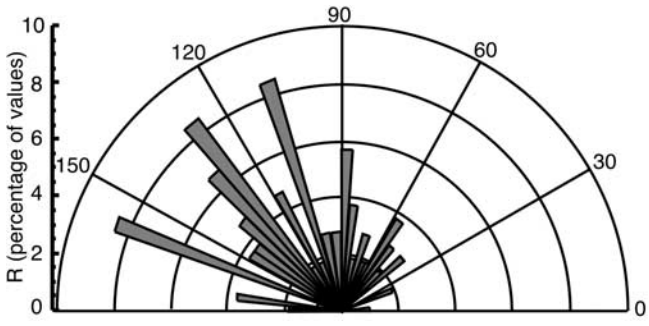

Figure 6. Polar plot of yardang directions from MOC images, including bidirectional fields, from 155 MOC images in the MFF. Most of the yardangs tend to point northwest-southeast, but orientation directions vary widely.

however, it does not account for the large distance between valleys or the shallow regional gradient in the MFF. We also find no evidence for deposition in valley floors, which should be present had intense erosion occurred. Even with extensive erosion, we would still expect to see some evidence for layering within this region of the MFF. However, MOC and MOLA evidence indicate that the MFF in the ridge and valley region, which is most similar to polar deposits in overall appearance, is massive at all currently available resolutions. Elsewhere in the MFF, we find localized evidence for some small-scale layering in MOC images; however, these regions are wholly unlike polar layered terrain in MOLA topography and larger-scale images. Our conclusions here support the independent argument by *Tanaka* [2000] that a polar origin is unlikely on the basis of timescales necessary for polar wander.

3. Layering Elsewhere Within the MFF

[15] Although the ridge and valley region of the MFF lacks readily identifiable layers, elsewhere, MOC images reveal some small-scale layers, and MOLA topography shows the presence of thicker layers which are more pervasive throughout the formation. The layers identified in MOC and MOLA data are primarily at smaller scales than the previously mapped member thickness [*Scott and Tanaka*, 1982, 1986; *Greeley and Guest*, 1987] and are thus more numerous than those that the Viking data detected [*Zimbelman et al.*, 1998; *Bradley and Sakimoto*, 2001b].

[16] Layers are apparent in the MFF at three distinct scales. On the largest scale, layers can be seen in MOLA DEMs and Viking images. These layers are readily visible in MOLA passes, measure up to 400 m in thickness, and are continuous across tens of kilometers (Figure 5a). Of these the thickest layers are primarily in the region just east of Apollineras Patera. Several of these thicker layers were identified by *Scott and Tanaka* [1982]; however, MOLA topographic breaks indicate that these layers may be separated further. Medium-scale layering is apparent in the MFF in MOC images and, with careful analysis, in some MOLA passes (Figure 5b). These layers measure between 50 and 60 m in thickness and are continuous across at least hundreds of meters. The smallest scale of MFF layering is apparent only in MOC images and is not measurable using MOLA topography. These layers are <10 m thick and are continuous across at least hundreds of meters (Figure 5c). Elsewhere within the MFF are regions that appear massive in all available images as well as MOLA topography (see, for example, Figures 2 and 4). It is possible that some layering is obscured by the ubiquitous yardangs or is not apparent because there is not a substantial change in resistance between layers. However, it seems likely that where small-scale layering exists it is relatively localized. In contrast, large-scale resistant layers cover hundreds of thousands of square kilometers in western sections of MFF (near Apollineras Patera and south of Elysium Mons).

4. Yardang Orientations

[17] Layering in some regions of the MFF appears to be expressed and/or emphasized by changing yardang orientations. These have been suggested to indicate multiple stages of deposition and eolian erosion [*Wells and Zimbelman*, 1997; *Zimbelman et al.*, 1998]. In order to investigate the range of yardang orientations, we surveyed 155 released MOC images of the MFF between 140° and 240°E and 15°S and 15°N. Using sinusoidally projected images, we measured the trend direction of the central axis of multiple yardangs within these images. If several similar angles existed within a single image, the average was used. Many of the images also contain bidirectional yardangs, where axes trend in two distinct directions. In these cases both directions were measured.

[18] Yardangs trend in a wide variety of directions. The most common is NW-SE, a direction consistent with the overall shape of the MFF outcrops, but angles vary considerably, and several regions of NE-SW, E-W, and N-S trending yardangs also exist (Figure 6). Yardang orientation could be affected by a wide variety of factors, including wind direction, local topography, and MFF material properties. If wind were the only factor involved in yardang orientation, we would expect local to regional consistency

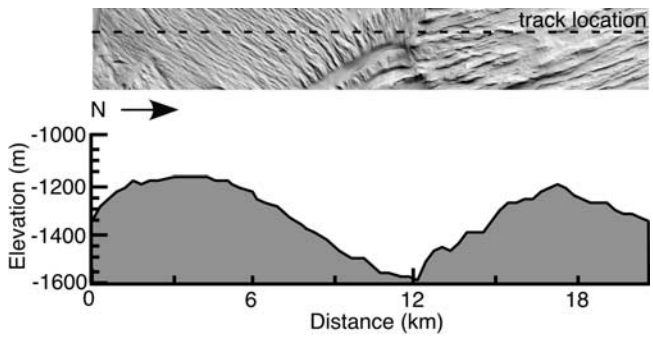

Figure 7. MOC image M0202832 shows changing yardang directions within the MFF. The image is centered at 11.92°S, 179.97°E and has a resolution of 5.69 m/pixel. The deep northwest trending grooves appear to postdate northeast trending yardangs, but their relationship with northwest trending yardangs is ambiguous. Yardangs also appear to rotate to align with the valley, indicating that wind might be channeled through local topographic lows. The graph contains MOLA pass 11235 at a vertical exaggeration of 10. Illumination is from the southwest. (MOC image courtesy of NASA/JPL/MSSS.)

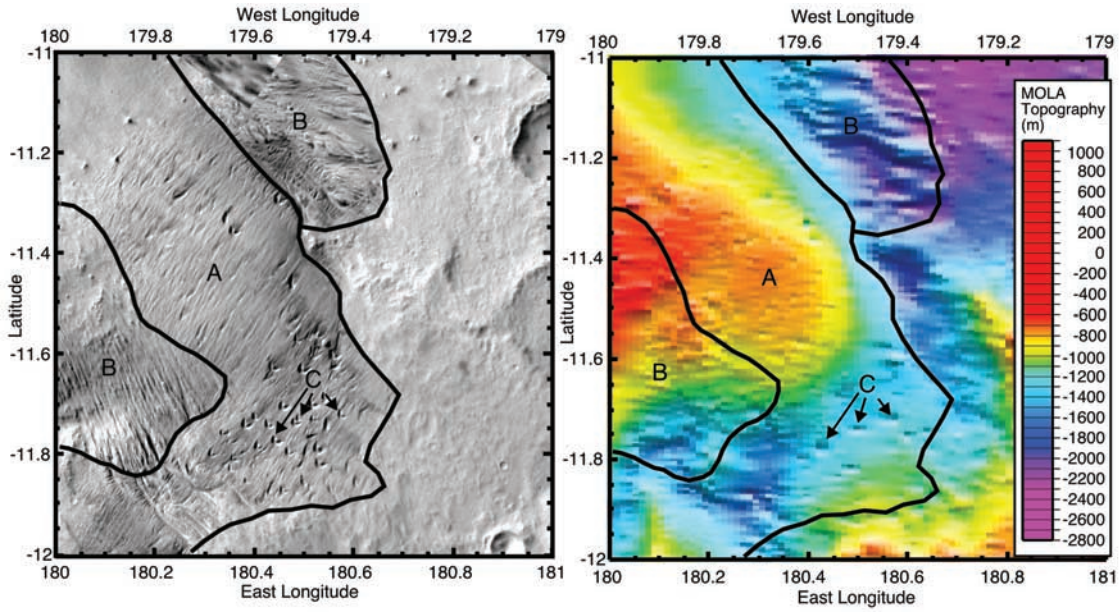

Figure 8. Viking high-resolution images 437S03 and 438S02 with resolution 68 m/pixel are overlaid on an MDIM with resolution 234 m/pixel. MOLA DEM shows the same area with resolution 64 pixels/degree longitude, 256 pixels/deg latitude using data through March 2001. (A) Northeast trending yardangs. (B) Northwest trending yardangs. (C) V-shaped depressions.

of axis orientation within the topmost set of yardangs. If underlying topography controlled their formation, the yardangs would have a consistent orientation relative to local slope. We do not observe a consistent orientation regionally or relative to topography; however, the yardangs do intersect at a consistent angle when more than one trend occurs. This suggests that material properties within the MFF, such as jointing, may control yardang orientation.

[19] In most cases the MOC images are widely spaced, making it difficult to interpret the spatial relationship between localities that might be subject to similar local wind regimes. However, we found one example near 179°–183°E and 10°–13°S where high-resolution Viking images combined with MOC images show in detail the boundary between a set of NW and NE trending yardangs. The boundary between the two yardang directions is abrupt. Yardangs approaching the boundary intersect at nearly 90° angles with little or no change in trend (Figure 7). In some areas there appears to be some streaking or overprinting of NW yardangs or wind streaks on top of NE trending ones, but this effect is very localized. In Figure 7 the change in yardang direction occurs at a distinct low in the topography. Elsewhere, the change occurs in the middle of a slope (Figure 8). Yardangs oriented in perpendicular directions occur within the same elevation range throughout this region, and while a suggestion of superimposed layers of yardangs oriented in different directions seems a particularly poor fit to the observations here, we have no other satisfactory explanation for their orientations relative to the local topography.

[20] Another interesting feature found in this region are large V-shaped depressions. These depressions are aligned with yardangs but are distinct in images and are about twice the amplitude and nearly twice the wavelength. Dozens exist between 180° and 181°E and 11° and 12°S and several more are found near 205°E, 2°S. These depressions, previously identified by *Rhodes and Neal* [1981] and *Schultz and Lutz* [1988], form with their central axis parallel to yardang direction (Figures 8 and 9). The depressions range from 700 to 1500 m long and 100 to 200 m wide. MOLA

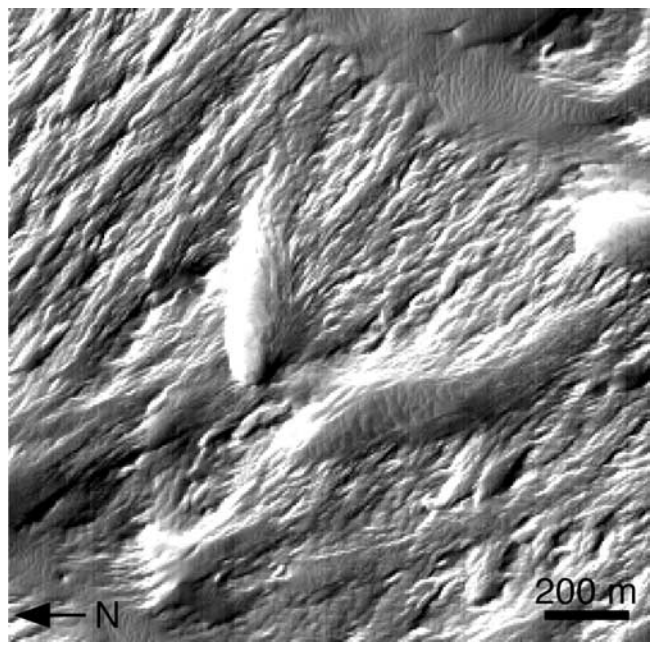

Figure 9. MOC image M0202382 of a V-shaped depression common in northeast trending yardang fields. To carve these flute-like shapes, the wind probably flowed from southwest to northeast. The image is centered at 11.92°S, 179.97°E. Illumination is from the southwest. (MOC image courtesy of NASA/JPL/MSSS.)

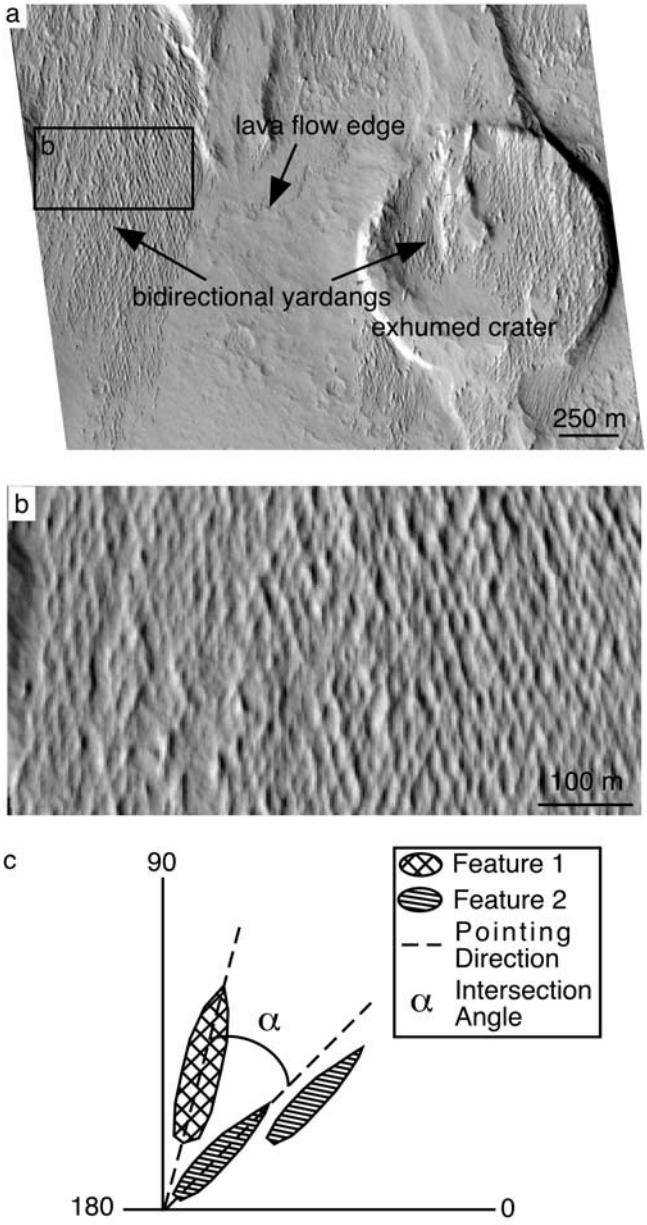

Figure 10. (a) MOC image M0801561 shows an example of bidirectional yardangs within the MFF. The image is centered at 7.42°N, 197.11°E and has a resolution of 1.46 m/pixel. The image also shows the edge of a lava flow underlying the MFF and an exhumed crater. (b) Yardangs in this image intersect at 41°. Illumination is from the southwest. (c) Cartoon of how intersection angle is measured from bidirectional features. (MOC image courtesy of NASA/JPL/MSSS.)

passes reveal a depth of 50–100 m. These features are found only in northeast trending yardangs in areas where the MFF appears to form a thin coating over the underlying basement material.

[21] Intersecting yardang trends like those in Figures 8 and 9 do not appear to be simply related to distinct layers within clear elevation ranges. It appears more likely that the variety of yardang directions expressed on the surface are a function of wind regimes, underlying topography, or structural differences. V-shaped depressions occur in only a few sections of northeast trending yardangs. They are most likely a result of less resistant material within those sections of the deposit being removed and leaving deflation hollows. The regular shape and alignment of the depressions indicate that they were probably formed by the same wind regime as surrounding yardangs.

5. Directional Trends of Yardangs

[22] One possible structural control on yardang directions could be the presence of joints within cohesive layers. This possibility is explored by searching for common yardang intersection angles, assuming that joint sets would tend to intersect at common angles but not necessarily be oriented in a consistent direction. Of the 155 MOC images we observed in the MFF region, 23% exhibited a characteristic bidirectional pattern formed by yardangs with axes trending in two distinct and apparently simultaneously formed directions as neither appears to overprint the other (Figure 10). Some bidirectional yardangs are also apparent in a few of the high-resolution Viking images and have been suggested to be a result of complementary joint sets in resistant layers of MFF [*Scott and Tanaka*, 1982]. *Tanaka and Golombek* [1989] later observed that common yardang intersection angles in Viking images may indicate a least principal stress direction of N70°E.

[23] In MOC images containing complementary yardang orientations, more than 70% had intersection angles between 30° and 45°, with the most common (24%) angle between 36° and 40° (Figure 11). The yardang orientation is plotted against the angle of intersection in Figure 11, supporting the observation that while there is a wide distribution of yardang axis orientations, the angle between bidirectional yardangs remains fairly consistent.

[24] The bidirectional quality is distributed widely throughout the MFF, occurring on both thin and thick deposits. Bidirectional yardangs occur throughout the MFF and do not correlate to latitude or elevation. MOC image M0703093 (Figure 12) shows the presence of several resistant blocky layers intersecting at ~40°. These features are reminiscent of columnar jointing and do not appear to be wind sculpted like nearby yardangs. The intersecting blocky layers are best attributed to localized joint patterns within the MFF. Interestingly, surrounding yardangs have axes that echo these joint orientations. Bidirectional yardangs in this MOC image are likely controlled by the jointed material observed in the blocky layer.

[25] As seen in Figure 6, yardangs within the MFF (both single and bidirectional) point in all possible directions but tend predominantly toward the northwest, a direction consistent with the lobate form of the MFF deposits. However, there is a wide variation in pointing direction of bidirectional yardang fields (Figure 11). They do not appear to have any correlation to wind flow, but they do maintain an average 40° intersection angle. Yardangs are eroded preferentially along zones of weakness, suggestive of joint planes. The lack of alignment of bidirectional fields indicates that principal stress directions are widely varied. Also, because there is no indication of similar jointing or lineations in material underlying the MFF, it is probable that joints were not tectonically derived.

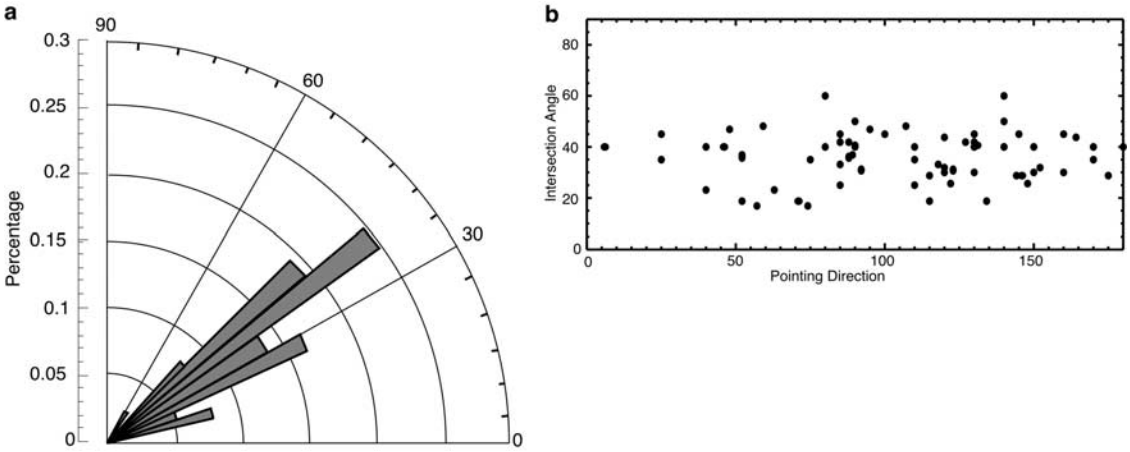

Figure 11. (a) Angles of intersection of 35 bidirectional yardang fields from MOC images in the MFF. Twenty-four percent of angles measure between 36° and 40°. (b) Plot of yardang axis pointing direction versus intersection angle for bidirectional yardangs. Yardang axes vary widely, while intersection angle tends to range between 30° and 45°.

[26] The most likely cause for nontectonic joints is cooling and contraction of an extrusive rock. Cooling joints are fairly common in tuffs and volcanic air fall deposits, where cracks tend to form at the surface and propagate downward through the formation shortly after deposition. Sedimentary rocks may also possess nontectonic joints formed by compaction and settling. However, sedimentary joints are primarily a result of burial and later uplift and are not likely associated with the MFF. Another possible source of the jointing is desiccation cracking; however, these types of cracks do not tend to show regular patterns of the type observed in the MFF [e.g., *Seyfert*, 1987; *Cas and Wright*, 1988]. We find cooling joints to be the most viable explanation for the bidirectional yardang pattern observed in the MFF.

[27] Since the MFF is presumably composed of the same type of material, why do we not see joint patterns throughout the entire formation? There are two possible explanations for this: first, that joints do not exist throughout the entire formation and, second, that wind direction was the stronger force on yardang trends in some areas. Joints may not have formed in some layers of the MFF because of increased layer thickness, changes in grain size, or differences in depositional temperature. This may explain why bidirectional yardang fields tend to be fairly common where the MFF forms a thin veneer on underlying material. In areas where joint patterns are roughly perpendicular to the dominant northwesterly wind direction, eolian excavation may not move preferentially along joints. This possibility is supported by the relatively small number of bidirectional

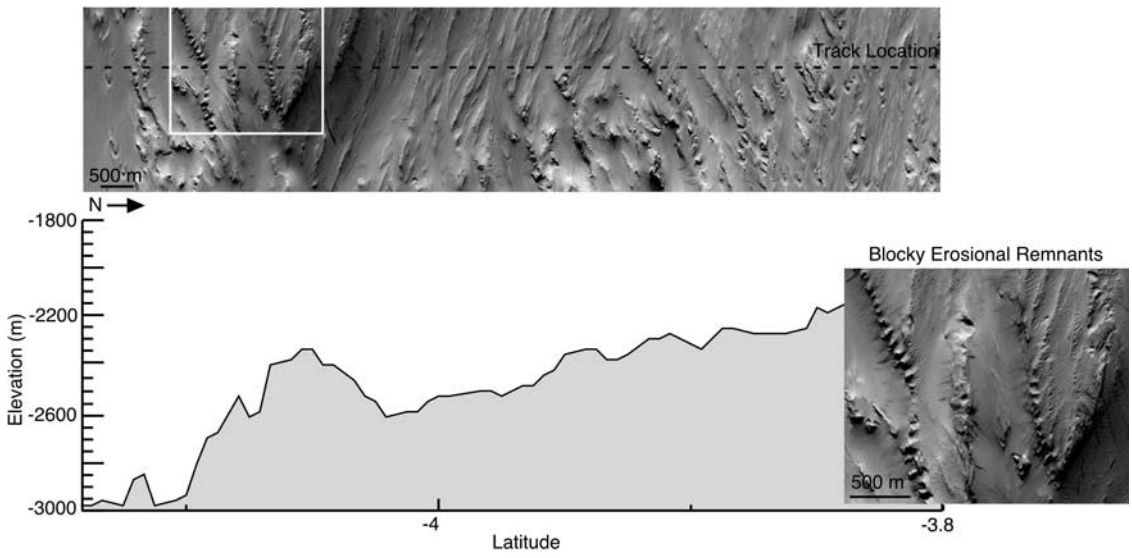

Figure 12. MOC image M0703093 showing blocky, resistant layers in the MFF. These layers intersect at 40° and may be indicative of jointing. The image is centered at 4.26°S, 200.2°E. MOLA orbit 12350 is shown below the image; the MOLA pass has a vertical exaggeration of 5. Illumination is from the southwest. (MOC image courtesy of NASA/JPL/MSSS.)

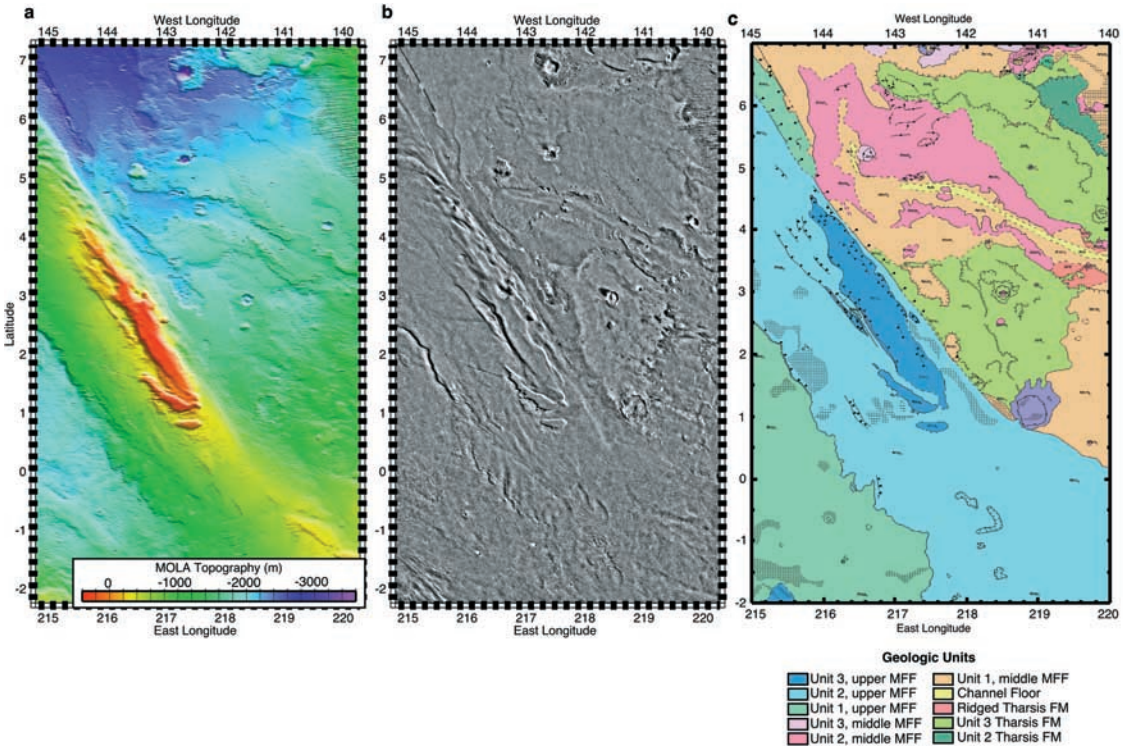

Figure 13. MOLA DEM of the base of Arsia Mons with geologic map (a) MOLA DEM with resolution of 64 pixels/degree of MFF interaction with fluvial channels at the base of Arsia Mons. (b) Viking MDIM with resolution of 256 pixels/degree. (c) Geologic map with 1:4M resolution showing location of the fluvial channel. After *Zimbelman et al.* [1996b, 1998].

yardangs oriented between 0° and 40° ENE (see Figure 11), the direction perpendicular to dominant wind flow.

6. Fluvial Interaction With the Medusae Fossae Formation

[28] While yardangs, a classic result of eolian removal of friable material, are one of the defining characteristics of the MFF, wind may not be the only erosive force acting on the deposit. Recent discoveries using MOC have revealed the presence of sapping on many surfaces of Mars, indicating that recent fluvial activity at or near the surface is a real possibility [*Malin and Edgett*, 2000a, 2000b]. MOLA data combined with a reexamination of published geologic mapping relationships may suggest large-scale fluvial erosion of the MFF region predating Hesperian time [*Dohm et al.*, 2001].

[29] Viking images alone do not reveal any fluvial interaction with the MFF. However, MOLA data show the presence of 150–900 m deep channels carved into basement material beneath the MFF in several areas [*Zimbelman et al.*, 2000; *Bradley and Sakimoto*, 2001a]. *Zimbelman et al.* [2000] mapped a fluvial channel west of Arsia Mons (Figure 13) that appears to crosscut part of the MFF, indicating that water may have eroded the MFF locally. 1:500,000 scale geologic mapping by *Zimbelman et al.* [1996a] of eastern MFF deposits shows a complex relationship between Arsia lava flows, the MFF, and fluvial channels (Figure 13). The channel location is flanked by lava flows previously interpreted as pepperites, a lava emplaced in wet sediments [*Gregg and Schultz*, 1997]. The presence of this channel may indicate that channelized flow existed on the Martian surface as recently as the late Amazonian.

[30] Southeast of Nicholson crater the MFF overlies an extensive channel system (Figure 14). Labou Vallis branches away from Mangala Vallis and is truncated by a large lobe of MFF. There is no indication in this region of substantial water flow after the MFF was deposited. The floors of Labou Vallis and several smaller channels originating in the highlands are coated by MFF yardangs (Figure 15). Additionally, MOLA topography reveals that the edge of the MFF deposit fills the bottom of Labou Vallis with at least 100 m of material along a 30 km section of the channel at 7.25°S between 202.5° and 203°E [*Bradley and Sakimoto*, 2001a]. Thus it appears that the MFF was deposited after the fluvial activity ceased in this region.

[31] Several low valleys occur within the MFF trending NNW between Labou Vallis and the plains surrounding Nicholson crater. MOC images do not show any indication of surface flow through these valleys; it is probable that they are a result of MFF draped over preexisting channels. The regional gradient supports a northwesterly flow direction from the highlands toward Nicholson crater, and channels in the basement material are clearly truncated at the edge of the MFF.

[32] Two of the valleys within the MFF east of Nicholson crater are considerably wider and deeper than would be expected for MFF material draped over a preexisting channel, assuming that Labou Vallis was the source for

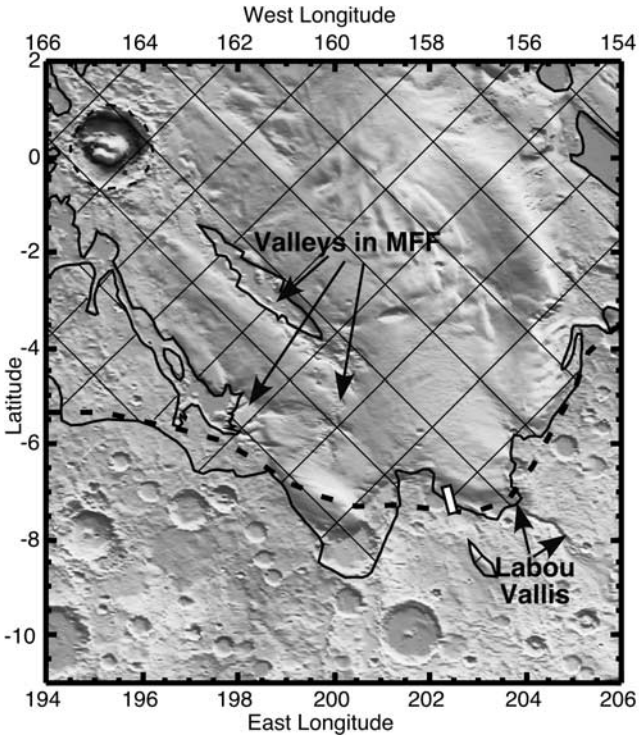

Figure 14. Context MOLA shaded relief map with resolution 64 pixels/degree of MFF interaction with local fluvial channels. In this region there is no indication of channel flow after MFF deposition. The white rectangle indicates MOC M0806902 (Figure 19). Solid lines are MFF boundaries mapped by *Zimbelman et al.* [2000]. Hash marks indicate MFF deposits. The dashed line is the approximate location of the dichotomy boundary.

that channel and that the channel cross-sectional area remained relatively constant. These valleys are 20 km wide and 500–800 m deep, compared to Labou Vallis, which is also 20 km wide but only 150–200 m deep. Because the valleys happen to run parallel to the dominant wind direction of northwest (based on yardang orientation) in this region, they contain yardangs 5–10 times the size of those found elsewhere in the MFF. Average MFF yardangs range from 10 to 40 m in height, while those found in this valley reach 200 m (Figure 16). One explanation for the increased depth of these valleys compared to Labou Vallis could be that wind preferentially excavated the MFF deposited in the topographic low over preexisting channels.

[33] MOLA topography suggests that prior to MFF deposition, Labou Vallis may have been the source for an extensive channel network originating in the Noachian highlands and flowing into the plains surrounding Nicholson crater (Figure 17). The MFF was later deposited on top of this channel system, coating both highland and lowland areas across the dichotomy boundary. There is no evidence for water flow through these channels after MFF deposition. Rather, wind seems to be the dominant recent erosional force in the region and probably continues to deepen valleys in the MFF located over preexisting channels.

7. Area and Volume Measurements for the MFF

[34] The MFF region is one of the areas on Mars with substantial changes in mapped topography between the pre-MGS and the MGS data sets (see Figure 1). These differences greatly affect volumetric estimates for the MFF even without changing anything else, such as unit boundaries. Therefore we have reestimated the MFF volume on the basis of the previously mapped unit boundaries. Additionally, MOC image coverage shows thin coatings of yardangs locally draped over areas not previously mapped as MFF. We have estimated a maximum possible extent on the basis of their distribution.

7.1. Methods

[35] Area and volume of the MFF were calculated using GMT version 3.3.6. This program takes a gridded topo-

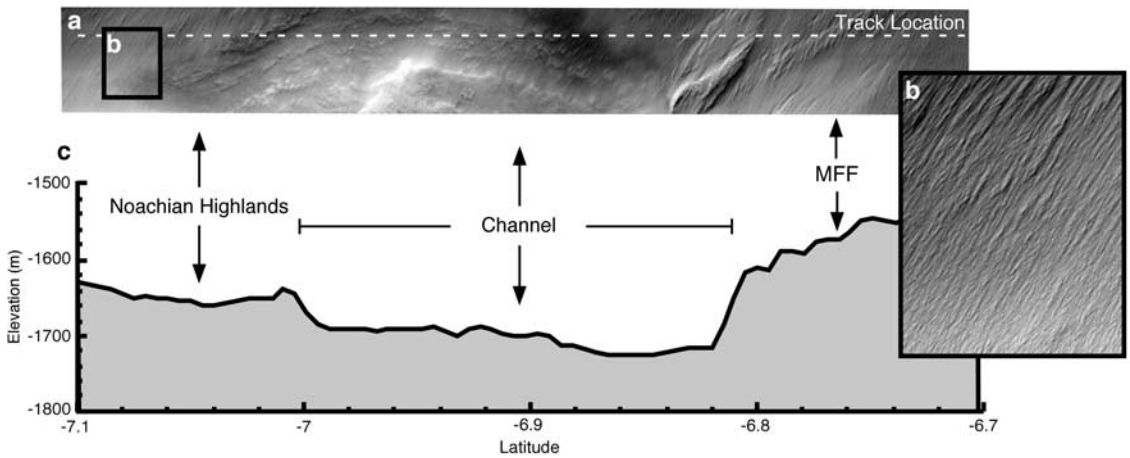

Figure 15. Yardangs coating Labou Vallis (a) MOC image M0806902 of Labou Vallis and nearby highlands coated with MFF. The image is centered at 201.88°E, 7.47°S and has a resolution of 7.15 m/pixel. Illumination is from the southwest. (b) Enlarged section of image M0806902 showing yardangs coating the highland terrain. (c) MOLA pass 12851 corresponding to the MOC image. The pass has a vertical resolution of 20. (MOC image courtesy of NASA/JPL/MSSS.)

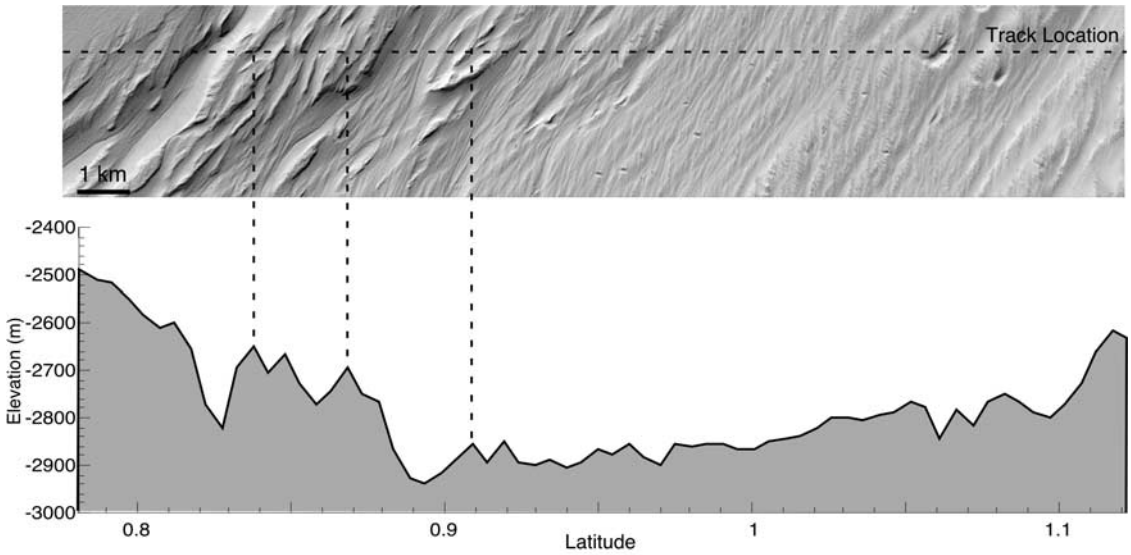

Figure 16. Large yardangs in a MFF valley. MOC image M0801559 is centered at 197.93°E, 1.01°N and has a resolution of 4.34 m/pixel. Corresponding MOLA pass 12852 reveals that some yardangs are 150 m high (elsewhere in the MFF, yardangs average 10–40 m high). The pass has a vertical exaggeration of 10. Illumination is from the southwest. (MOC image courtesy of NASA/JPL/MSSS.)

graphic map created using MOLA data and measures the area and volume of material above a specified contour level. The MFF deposits were divided into six sections ranging from 139° to 231°E and measured separately (Table 2). Boundaries for volumetric calculation were distinguished by comparing geologic maps [*Scott and Tanaka*, 1986; *Greeley and Guest*, 1987] to the changing topographic signature between the MFF and underlying units. In MOLA DEMs the MFF tends to form large, cohesive lobes often with considerable scarps at contacts with underlying units. Where the MFF overlies the dichotomy boundary, we broke the formation into smaller sections and

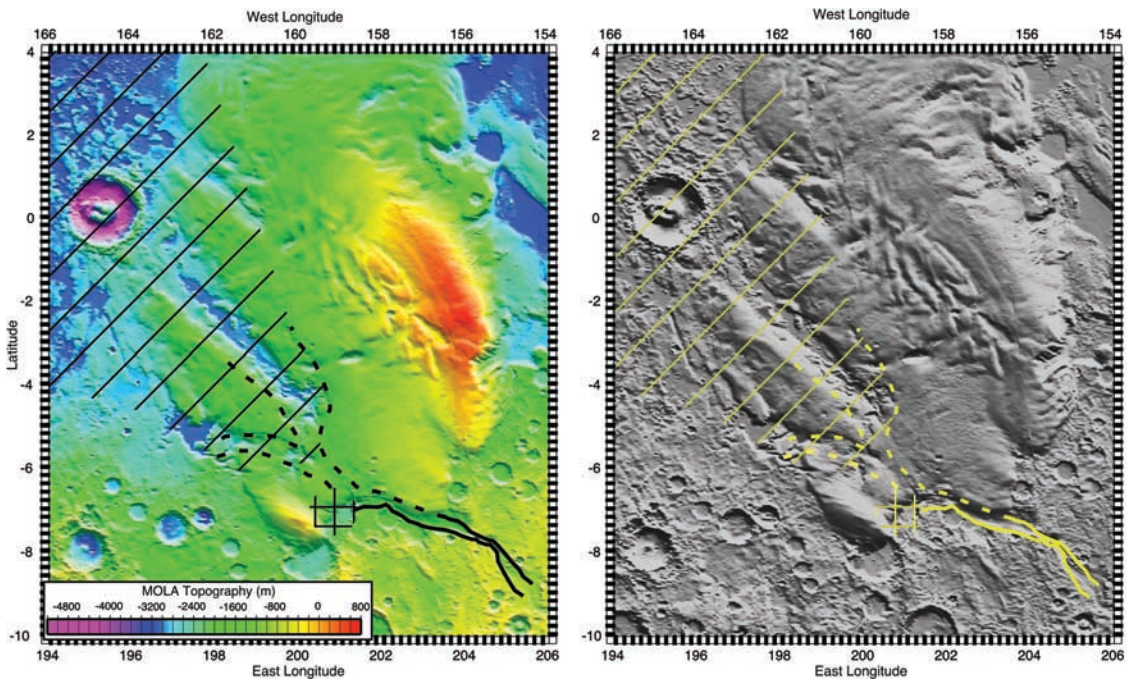

Figure 17. (left) MOLA color DEM and (right) shaded relief map of the MFF north of Labou Vallis. DEMs have a resolution of 256 pixels/degree latitudinally and 64 pixels/degree longitudinally. The solid line indicates where Labou Vallis is currently visible; the dashed lines are probably locations for buried channels. The hatched region is a possible ponding area. Slashes indicate the probably outflow region of water from the channel system.

Table 2. MFF Area and Volume Calculations

MFF Coordinates	Basal Elevation, m	Area, km^2	Volume, km^3
	Section 1		
1°–5°N, 139°–142°E	−2700	31,000	7000
2°S–4°N, l42°–156°E	−2700	242,000	84,000
2°–6°S, 147°–157°E	−2700	137,000	75,000
	Section 2		
7°S–0°N, 166°–176°E	−2800	92,000	21,000
12.5°S–2°N, 179°–187°E	−2400[a]	106,000	67,000
11°S–2°N, 176°–179°E	−2400[a]	229,000	224,000
7°S–0°N, 187°–190°E	−2800	63,000	50,000
7°–9°S, 187°–188°E	−2000	4000	3000
	Section 3		
4°–13°N, 197°–204.5°E	−3200	128,000	61,000
3°S–4°N, 191°–210°E	−3200	418,000	377,000
3°–5°S, 192°–200.5°E	−3200	59,000	44,000
3°–7°S, 200.5°–205°E	−1500	54,000	36,000
5–8°S, 198.5–200.5°E	−1500	6000	3000
	Sections 4–5		
4°S–12°N, 210°–220°E	1000[b]	240,000	135,000
	Section 6		
0°–10°N, 220°–231°E	−1000[b]	289,000	178,000
Total		**~2,100,000**	**~1,400,000**

[a] Basal elevation was estimated assuming a constant slope across the dichotomy.
[b] Basal elevation derived from a detrended DEM.

chose basal elevations on the basis of apparent MFF boundaries (Figure 18). Eastern regions, which overlie Arsia Mons lava flows, were detrended to remove underlying slope.

7.2. Volume Calculation

[36] MOLA data suggest that the MFF covers an area of 2.1 × 10^6 km^2 and contains 1.4 × 10^6 km^3 of material. This calculation is approximately equal to that estimated by *Scott and Tanaka* [1982]; however, the volume is less than half the previous value. This discrepancy probably results from an overestimation of MFF thickness and depth of infill of some buried craters in pre-MOLA topography (see Figure 1). The volume is slightly larger than *Tanaka*'s [2000] estimate of 1 × 10^6 km^3, which used aerobraking data alone. This is likely a function of better resolution with the additional topographic data now available.

[37] As mentioned above, the MOC images have revealed that MFF-like materials form a thin coating on much of the area between major MFF outcrops. A survey of released MOC images reveals the presence of MFF-style yardangs far from topographically thick deposits of MFF, including several deposits southwest of Arsia Mons (Figure 19). The presence of yardangs between thick MFF deposits strongly suggests that the formation was once far more extensive than at present. The total area potentially once coated by the MFF is approximately 5 × 10^6 km^2, determined by summing all the area containing yardangs shown in Figure 19. However, because the additional yardang coating seen in images is not thick enough to be obvious in MOLA DEMs, the additional volume of these yardangs probably is insignificant compared to the total volume of the MFF. It is interesting that some of the yardangs and MFF material may be within, on top of, and partially buried by young Cerberus Fossae volcanics. This lends some credence to *Keszthelyi et al.*'s [2000] suggestion that the MFF is the pyroclastic component of those extensive flow deposits.

8. Discussion

[38] The observations outlined here have interesting implications when we consider the nature and origin of the MFF. The lack of horizontal layering, particularly widespread layering, significantly reduces the likelihood of carbonate platforms, shoreline, and other assorted aqueous-related origins of deposits, as does the lack of spectral signature for carbonates on Mars [*Bandfield et al.*, 2000]. For the reasons discussed earlier we also consider polar deposits unlikely. This is further supported by the geodynamic difficulties of a rotational pole change late in Mars' history [e.g., *Tanaka*, 2000]. This leaves us with three remaining plausible possibilities: ignimbrites and

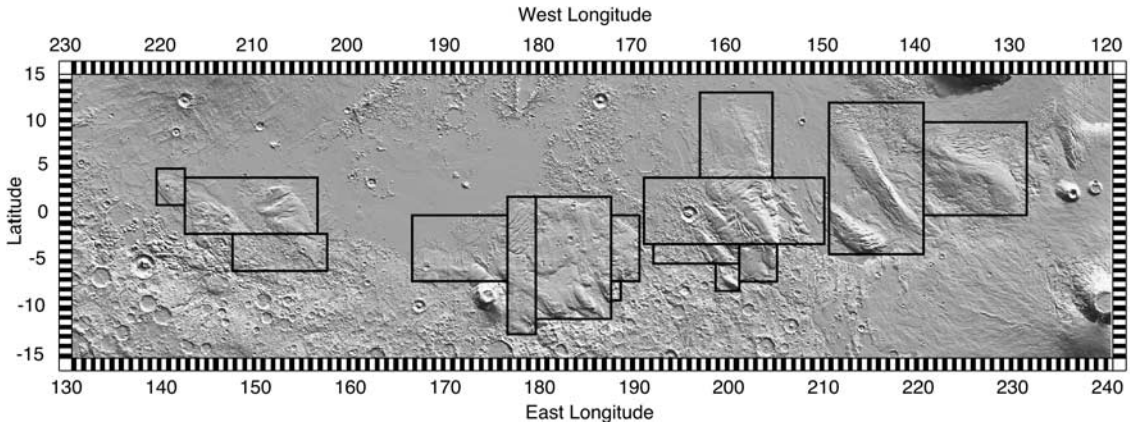

Figure 18. Boundaries of area/volume calculations on DEM. The outlined boxes indicate areas measured in area/volume calculations. Basal elevations used for these calculations are found in Table 2. The underlying image is a MOLA DEM with resolution 32 pixels/degree longitude by 64 pixels/degree latitude using data through January 2001.

Table 3. Comparison of Material Attributes

Property	Medusae Fossae Formation	Ashfall Tuff	Ignimbrite	Eolian Materials (Nonvolcanic)
Horizontal or near-horizontal layering	yes (discontinuous)	yes, in either cooling or eruption units	yes, in either cooling or eruption units	sometimes
Jointing	yes	yes, in welded portions	yes, in welded portions	no, unless cemented by subsequent fluvial or other activity
Layers or zones of variable resistance to weathering (horizontal or otherwise)	yes	yes, in partially common welded tuffs	common	rare, unless cemented by subsequent fluvial or other activity
Upper flat surfaces	no (obvious subsequent erosion)	sometimes	common	sometimes
Mantles topography	yes	yes	sometimes, but most commonly fills valleys	yes
Steep primary dips	possibly	yes	no	no
Yardangs	common	common	common	uncommon

similar pyroclastic flow deposits, volcanic air fall deposits (such as ashes and tuffs and co-ignimbrite ashfalls), and nonvolcanic eolian deposits such as loess.

[39] Table 3 compares properties found in the MFF with those in terrestrial examples of the materials proposed above. For example, the MFF commonly mantles topography, and features such as lava flows and fluvial channels can be detected in the topography even though they are clearly covered by MFF materials. Mantling behavior is more typical of air fall deposits than ignimbrites. Ignimbrites tend to preferentially fill valleys first and leave a thinner veneer on high ground [*Compton*, 1985; *Cas and Wright*, 1988; *Fisher and Schmincke*, 1984]. Joint sets are a common result of cooling in both ignimbrites and ashfall tuffs. Because joints do not appear to be tectonically related, it is more difficult to explain jointing if the material is eolian. However, if an eolian deposit were well indurated, joints could occur as a result of compaction or cementation of material. This mode of joint formation is less likely as it requires a consolidated material and is not common without tectonic stresses [*Seyfert*, 1987].

[40] Steep primary dips result when materials are emplaced over existing topography, and the bedding follows that topography. For MFF the bedding often appears to echo underlying topography, but so far it has been quite difficult to determine if the MFF materials follow the original slope closely or if they simply reflect but significantly reduce their magnitudes. Both properties may in fact be present, and this may suggest either that the MFF is a mix of related volcaniclastic deposits (ignimbrite and co-ignimbrite ashfalls, for example) or that secondary failure of oversteepened primary deposits has been a factor (as might be expected for extensive ashfall deposits on existing slopes).

[41] Layering or differential resistance to erosion is clearly demonstrated in the MFF at several scales. The local to regional character of the layering suggests multiple depositional episodes and/or laterally varying material properties. This is quite common in welded or partially welded ignimbrites or ashfall tuffs, and while it is not necessarily common in eolian deposits, it could conceivably be produced in eolian deposits with secondary alteration or cementation. If it is a partially indurated eolian deposit not of volcanic origin, the local resistant layers

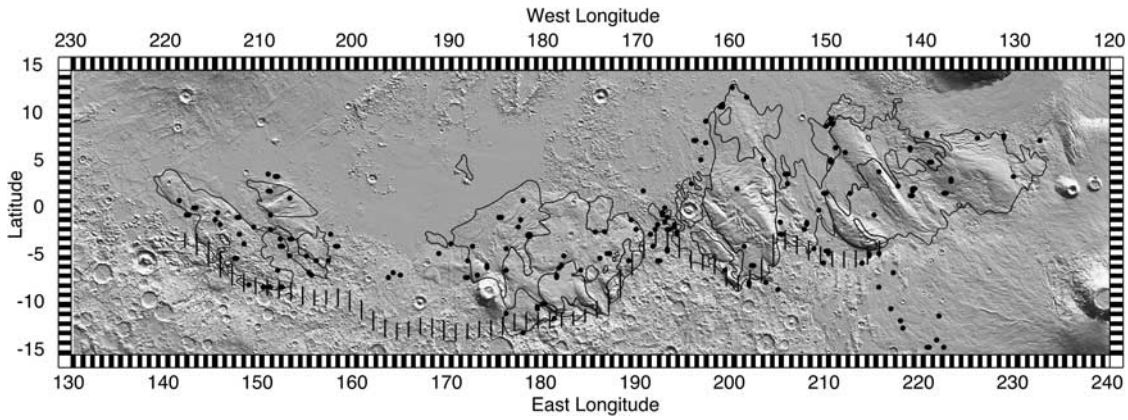

Figure 19. Location of MOC images with yardangs and dotted boundary of possible previously coated area. This image shows a MOLA shaded relief map overlaid with MFF boundaries from global geologic maps [*Scott and Tanaka*, 1986; *Greeley and Guest*, 1987]. The vertical dashes indicate the dichotomy boundary. Black dots are locations of MOC images containing yardangs of probable MFF composition; the location of yardangs suggests that the MFF may be more extensive than previously thought.

would have to be explained by compaction and perhaps accompanying fluid-related weathering and cementation.

9. Conclusions

[42] From this study we observe the following characteristics of the MFF:

1. The MFF has resistant zones or layers on several scales that are continuous locally to regionally but not formation-wide.

2. The MFF tends to drape over preexisting topography, following its contours. Examples of underlying topography include both lava flows and channel systems.

3. In some areas, resistant layers of MFF display complementary jointing. Orientations of the yardang axes are not consistent, but the characteristic angles within the joint sets are. Spacing of joints appears to be regular locally but was not quantitatively assessed in this study.

4. The MFF contains many yardangs, suggesting a somewhat friable material. The orientations of their axes are independent of elevation or any layering in some locations and vary with layering/elevation changes in others.

5. The MFF's upper surface is not flat and displays significant evidence of eolian erosion.

6. Resistant layers appear to be planar locally (on MOC scales), but not necessarily horizontal.

[43] Mars Global Surveyor has revealed the Medusae Fossae Formation to be a somewhat different deposit than was thought from the Viking data. We find new evidence for layering on multiple scales, discontinuous resistance to erosion, topographic mantling, possible jointing, greater pre-erosion extent, relationships with nearby volcanic flows, and extensive eolian erosion. We suggest that a volcanic air fall deposit is most consistent with all of these observations. However, we cannot rule out nonvolcanic eolian deposits, pyroclastic flow (instead of fall), or mixed volcanic flow and fall deposits completely.

[44] **Acknowledgments.** This work would not have been possible without the assistance of Jim Roark and Greg Neumann with data processing, grid routines, visualization, and software tools. Peter Neivert was a tremendous help with figure preparation. We thank the MOLA Science Team for ongoing discussions, encouragement, and support and Ken Tanaka and an anonymous reviewer for their insightful comments and suggestions. This work was done under NASA Mars Data Analysis Program grants NAG5-8565 and NAG5-11150 to S.E.H.S. and partial funding of B.A.B. by D. Smith and J. Garvin of MOLA Science Team. The geologic mapping of J.R.Z. was supported by a grant from NASA's Planetary Geology and Geophysics Program.

References

Bandfield, J. L., V. E. Hamilton, and P. R. Christensen, A global view of Martian surface compositions from MGS-TES, *Science*, *287*(5458), 1626–1630, 2000.

Bradley, B. A., and S. E. H. Sakimoto, Investigation of parallel valleys in the Medusae Fossae Formation south of Marte Valles, *Geol. Soc. Am. Abstr. Programs*, abstract 51,071, 2000.

Bradley, B. A., and S. E. H. Sakimoto, Relationships between the Medusae Fossae Formation (MFF), fluvial channels and the dichotomy boundary southeast of Nicholson Crater, Mars, *Proc. Lunar Planet. Sci. Conf. 32nd*, abstract 1335, 2001a.

Bradley, B. A., and S. E. H. Sakimoto, Layers and jointing within the Medusae Fossae Formation, Mars, *Eos Trans. AGU*, *82*(20), Spring Meet. Suppl., P41-A02, 2001b.

Bradley, B. A., E. B. Grosfils, and S. E. H. Sakimoto, Boundaries and stratigraphy of the Medusae Fossae Formation and Elysium Basin materials using Mars Orbiter Laser Altimeter, *Proc. Lunar Planet. Sci. Conf. 31st*, 2055–2056, 2000.

Cas, R. A. F., and J. V. Wright, *Volcanic Successions, Modern and Ancient: A Geological Approach to Processes, Products and Successions*, 528 pp., Chapman and Hall, New York, 1988.

Compton, R. R., *Geology in the Field*, 398 pp., John Wiley, New York, 1985.

Dohm, J. M., et al., Latent outflow activity for western Tharsis, Mars: Significant flood record exposed, *J. Geophys. Res.*, *106*(E6), 12,301–12,314, 2001.

Edgett, K. S., B. J. Butler, J. R. Zimbelman, and V. E. Hamilton, Geologic context of the Mars radar "Stealth" region in southwestern Tharsis, *J. Geophys. Res.*, *102*(E9), 21,545–21,567, 1997.

El-Baz, F., C. S. Breed, M. J. Grolier, and J. F. McCauley, Eolian features in the western desert of Egypt and some applications to Mars, *J. Geophys. Res.*, *84*(B14), 8205–8221, 1979.

Fisher, R. V., and H. U. Schmincke, *Pyroclastic Rocks*, 472 pp., Springer-Verlag, New York, 1984.

Forsythe, R. D., and J. R. Zimbelman, Is the Gordii Dorsum escarpment on Mars an exhumed transcurrent fault?, *Nature*, *336*, 143–146, 1988.

Greeley, R., and J. E. Guest, Geologic map of the eastern equatorial region of Mars, *U.S. Geol. Surv. Misc. Invest., Map I-1802-B*, 1:15,000,000, 1987.

Gregg, T. K. P., and P. H. Schultz, Shallow Martian "sills": Intrusions or extrusions, *Proc. Lunar Planet. Sci. Conf. 28th*, 463–464, 1997.

Hartmann, W. K., and D. C. Berman, Elysium Planitia lava flows: Crater count chronology and geological implications, *J. Geophys. Res.*, *105*(E6), 15,011–15,025, 2000.

Head, J. W., Ancient polar deposits in the equatorial region of Mars: Tests using MOLA data, *Eos Trans. AGU*, *81*(19), *Spring Meet. Suppl.,* P42A-10, 2000.

Keszthelyi, L., A. S. McEwen, and T. Thordarson, Terrestrial analogs and thermal models for Martian flood lavas, *J. Geophys. Res.*, *105*(E6), 15,027–15,049, 2000.

Lanagan, P. D., A. S. McEwen, L. P. Keszthelyi, and T. Thordarson, Rootless cones on Mars indicating the presence of shallow equatorial ground ice in recent times, *Geophys. Res. Lett.*, *28*(12), 2365–2367, 2001.

Malin, M. C., Mars: Evidence of indurated deposits of fine materials, *NASA Conf. Publ. 2072*, 54, 1979.

Malin, M. C., and K. S. Edgett, Evidence for recent groundwater seepage and surface runoff on Mars, *Science*, *288*(5475), 2330–2335, 2000a.

Malin, M. C., and K. S. Edgett, Sedimentary rocks of early Mars, *Science*, *290*, 1927–1937, 2000b.

Malin, M. C., and K. S. Edgett, Mars Global Surveyor Mars Orbiter Camera: Interplanetary cruise through primary mission, *J. Geophys. Res.*, *106*(E10), 23,429–23,570, 2001.

Mouginis-Mark, P., The influence of oceans on Martian volcanism, *Proc. Lunar Planet. Sci. Conf. 24th*, 1021–1022, 1993.

Neumann, G. A., D. D. Rowlands, F. G. Lemoine, D. E. Smith, and M. T. Zuber, Crossover analysis of Mars Orbiter Laser Altimeter data, *J. Geophys. Res.*, *106*(E10), 23,753–23,768, 2001.

Parker, T. J., A comparison of the Martian Medusae Fossae Formation with terrestrial carbonate platforms, *Proc. Lunar Planet. Sci. Conf. 22nd*, 1029–1030, 1991.

Rhodes, D. D., and T. Neal, Crescent-shaped pits on Mars, *NASA Tech. Memo. 84211*, 232–234, 1981.

Rice, J. W., Jr., Elysium Basin, Mars: An intermittent or perennial lake from Noachian to Amazonian, in *Conference on Early Mars*, *LPI Contrib. 916*, p. 68, Lunar and Planet. Inst., Houston, Tex., 1997.

Sakimoto, S. E. H., H. V. Frey, J. B. Garvin, and J. H. Roark, Topography, roughness, layering and slope properties of the Medusae Fossae Formation from Mars Orbiter Laser Altimeter (MOLA) and Mars Orbiter Camera (MOC) data, *J. Geophys. Res.*, *104*(E10), 24,141–24,154, 1999.

Schultz, P. H., and A. B. Lutz, Polar wandering of Mars, *Icarus*, *73*(1), 91–141, 1988.

Scott, D. H., and K. L. Tanaka, Ignimbrites of Amazonis Planitia region of Mars, *J. Geophys. Res.*, *87*(B2), 1179–1190, 1982.

Scott, D. H., and K. L. Tanaka, Geologic map of the western equatorial region of Mars, *U.S. Geol. Surv. Misc. Invest., Map I-1802-A,* scale 1:15,000,000, 1986.

Seyfert, C. K., *The Encyclopedia of Structural Geology and Plate Tectonics*, pp. 359–369, Van Nostrand Reinhold, New York, 1987.

Smith, D. E., et al., The global topography of Mars and implications for surface evolution, *Science*, *284*(5419), 1495–1503, 1999.

Tanaka, K. L., Dust and ice deposition in the Martian geologic record, *Icarus*, *144*, 254–266, 2000.

Tanaka, K. L., and M. P. Golombek, Martian tension fractures and the formation of grabens and collapse features at Valles Marineras, *Proc. Lunar Planet. Sci. Conf. 19th*, 383–396, 1989.

Ward, A. W., Yardangs on Mars: Evidence of recent wind erosion, *J. Geophys. Res.*, *84*(B14), 814–816, 1979.

Wells, G. L., and J. R. Zimbelman, Extraterrestrial arid surface processes, in *Arid Zone Geomorphology: Process, Form and Change in Drylands*, 2nd ed., edited by D. S. G. Thomas, pp. 659–690, John Wiley, New York, 1997.

Zimbelman, J. R., D. Crown, and D. Jenson, Initial investigation of the enigmatic massive deposits in Amazonis Planitia, Mars, *Proc. Lunar Planet. Sci. Conf. 27th*, 1495–1496, 1996a.

Zimbelman, J. R., A. K. Johnston, and C. G. Lovett, Geologic map of the Medusae Fossae Formation within MTM quadrangle 05142 on Mars, *Geol. Soc. Am. Abstr. Programs*, *28*(7), A128, 1996b.

Zimbelman, J. R., D. A. Crown, J. A. Grant, D. M. Hooper, D. Black, and D. Blanchard, The Medusae Fossae Formation, Amazonis Planitia, Mars: Evaluation of proposed hypotheses of origin, *Lunar Planet. Sci*. [CD-ROM], *XXVIII*, abstract 1482, 1997a.

Zimbelman, J. R., A. K. Johnston, P. S. Russell, and C. G. Lovett, Regional geologic setting of the Medusae Fossae Formation on Mars, *Eos Trans. AGU*, *78*(46), Fall Meet. Suppl., F411, 1997b.

Zimbelman, J. R., A. K. Johnston, and S. D. Patel, Photogeologic constraints on the emplacement of the Medusae Fossae Formation, Mars, *Lunar Planet. Sci*. [CD-ROM], *XXIX*, abstract 1463, 1998.

Zimbelman, J. R., S. E. H. Sakimoto, and H. Frey, Evidence for a fluvial contribution to the complex story of the Medusae Fossae Formation on Mars, *Geol. Soc. Am. Abstr. Programs*, A50423, 2000.

Zuber, M. T., et al., Observations of the north polar region of Mars form the Mars Orbiter Laser Altimeter, *Science*, *282*, 2053–2060, 1998.

B. A. Bradley, Department of Geological Sciences, Brown University, Box 1846, Providence, RI 02912, USA. (Bethany_Bradley@brown.edu)

H. Frey, Geodynamics Branch, NASA Goddard Space Flight Center, Code 921, Greenbelt, MD 20771, USA. (frey@core2.gsfc.nasa.gov)

S. E. H. Sakimoto, GEST at the Geodynamics Branch, NASA Goddard Space Flight Center, Code 921, Greenbelt, MD 20771, USA. (sakimoto@core2.gsfc.nasa.gov)

J. R. Zimbelman, CEPS/National Air and Space Museum, Smithsonian Institution, MRC 315, Washington, D. C. 20560-0315, USA. (jrz@nasm.si.edu)